ACS APPLIED MATERIALS & INTERFACES

Letter

www.acsami.org

Unique Aspects of a Shape Memory Polymer As the Substrate for Surface Wrinkling

Junjun Li,[†] Yonghao An,[‡] Rui Huang,[§] Hanqing Jiang,[‡] and Tao Xie*,[†]

[†]Chemical Sciences & Materials Systems Laboratory Mail Code: 480-106-224, General Motors Research & Development Center, 30500 Mound Road, Warren, Michigan 48090-9055, United States

[‡]School of Mechanical, Aerospace, Chemical and Materials Engineering, Arizona State University, Tempe, Arizona 85287, United States

[§]Department of Aerospace Engineering and Engineering Mechanics, University of Texas, Austin, Texas 78712, United States

ABSTRACT: Typical bilayer wrinkle systems employ soft elastomers as the substrates. In contrast, shape memory polymers have recently emerged as attractive alternatives. Besides the shape fixing capability, shape memory polymers distinguish from elastomers in that they are rigid at room temperature, but experience significant modulus drop upon heating. We hereby report unique aspects of shape memory polymers as the wrinkle substrate utilizing a metallic thin film as the top layer. The feasibility to create both reversible and irreversible wrinkles (and diffraction colors) on a single substrate is demonstrated. Experimental conditions are identified to create crack free wrinkles and the impact of various experimental parameters on the wrinkle wavelength and amplitude is investigated. The results suggest that the wrinkle mechanics deviate notably from the existing theories established with elastomers as the wrinkle substrates. Thus, a new theory will need to be developed in the future, taking into account of unique thermomechanical properties of the shape memory substrate and possible plastic deformation of the thin film.

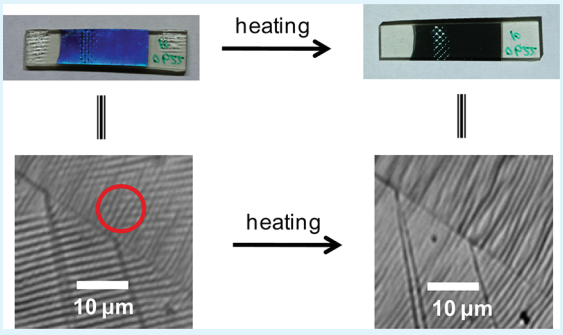

KEYWORDS: *surface wrinkling, shape memory polymer, structural color, thin film cracking, reversible colors*

INTRODUCTION

Surface wrinkles are encountered frequently in our daily lives, such as those on human skin and dehydrated apples. Whereas wrinkle formation may reflect unintended consequence of a natural process such as human aging, understanding and ultimately controlling wrinkle formation has emerged as an active research area.[1−10] Surface wrinkling occurs when a stiff thin film supported on a soft thick substrate is laterally compressed beyond a critical strain (ε_c) The lateral compression essential for the wrinkle formation is typically created via direct mechanical compression although other forms such as differential thermal expansion,[6] capillary force,[11] swelling,[12] and solvent diffusion[13] have also been explored. The commonly adopted linear elastic buckling theory predicts that the critical strain ε_c, the wavelength (λ), and amplitude (A) of the resulting wrinkles follow eqs 1−3.

$$\varepsilon_c = \frac{1}{4}\left[\frac{3(1-\nu_f^2)E_s}{(1-\nu_s^2)E_f}\right]^{2/3} \quad (1)$$

$$\lambda = 2\pi h\left[\frac{(1-\nu_s^2)E_f}{3(1-\nu_f^2)E_s}\right]^{1/3} \quad (2)$$

and

$$A = h\left[\frac{\varepsilon}{\varepsilon_c} - 1\right]^{1/2} \quad (3)$$

where E_f, E_s, ν_f and ν_s denote the Young's modulus of the thin film, the Young's modulus of the substrate, Poisson's ratio of the film, and Poisson's ratio of the substrate, respectively. h is the film thickness, and ε is the compressive strain.

Owing to its simplicity and low cost, surface wrinkling has emerged as an attractive microfabrication tool for controlling topography related material properties.[1,12,14−20] The quantitative correlations given by eqs 1−3, on the other hand, represent the basis for wrinkling based metrology,[2] such as the measurement of elastic moduli[21] and residual stresses[22] in thin films.

Equation 1 implies that a large contrast between E_f and E_s is essential for wrinkle formation at small strain levels. As such, elastomers are typically used as wrinkle substrates because of their low modulus (a few to tens of MPa), whereas the thin film can be a metallic layer, an oxide layer, or a rigid polymer. In addition, strains in an elastomer can be manipulated real time via simple mechanical stretching (or compression).[15,23] In the

Received: December 6, 2011
Accepted: January 10, 2012
Published: January 10, 2012

   dx.doi.org/10.1021/am201727a | ACS Appl. Mater. Interfaces 2012, 4, 598−603

absence of an external force, however, maintaining a certain strain in an elastomer is not possible. In contrast, shape memory polymers (SMPs) are capable of strain fixing without an external force.[24−27] Although typical SMPs are rigid (typical modulus around few GPa) at the room temperature, their moduli at elevated temperatures above the shape memory transition temperature are in line with those of elastomers. These features of SMPs make them uniquely attractive for use as wrinkle substrates.[17,19,20]

In particular, the strain fixing capability of SMPs can be utilized to create localized indents.[17] Although the indents themselves are compressive in nature, lateral tensile strains are created around their edges. After the deposition of a metallic thin film, the recovery of the tensile strain around the edge of the indents is triggered, leading to the lateral compression to the thin film and formation of localized wrinkles. The wrinkle structure and the highly reflective nature of the metallic thin film, in turn, give rise to diffraction based structural colors. In theory, mechanically induced elastic wrinkles are reversible via further mechanical manipulation that erases the compressive strain. The strain created via localized indents and the recovery, however, cannot be erased in any practical manner because of its nonuniaxial and inhomogeneous nature. As such, the wrinkle and the associated structural color are practically permanent. This is in sharp contrast to the reversible nature of wrinkles created via simple uniaxial stretching or compression.

Theoretically, the irreversible nature of the localized complex strains versus the reversible nature of uniaxial stains presents a unique opportunity to create both reversible and irreversible wrinkles (thus structural color) on a single substrate. Such feasibility is explored in this work. In addition, although SMP-based wrinkle systems have received increasing attention,[17,19,20] the associated mechanics are not well understood. In fact, limited data reported in the literature deviate noticeably from the classical theory of elastic buckling (eqs 1−3).[17,20] However, no reliable conclusion can be drawn because of the presence of structural defects (e.g., cracking and partial delamination) in the reported systems.[17,20] It is thus the further goal of this work to investigate the mechanics of the wrinkles in the absence of such defects. We should also note that although our particular interest lies in structure colors, the plasmonic effect associated with the structured metallic surface could be beneficial for a wide variety of applications.

EXPERIMENTAL SECTION

Materials. An epoxy SMP (T_g = 40 °C) was used as the wrinkle substrate. This epoxy SMP was obtained by the thermal curing (100 °C for 1 h and at 130 °C for 1 h) of an epoxy liquid mixture, which consists of an aromatic diepoxide (Dow 383, 3.6 g or 0.01 mol), an aliphatic diepoxide (Neopentyl glycol diglycidyl ether, 2.16 g or 0.01 mol), and an aliphatic diamine curing agent (Jeffamine D-230, 2.3 g or 0.01 mol). The sources of the epoxy liquid precursors, the detailed synthetic procedure, and the shape memory characteristics can be found in our previous publications.[17,28]

Wrinkle Formation. SMP samples were cut into rectangular strips (32 × 6 × 1 mm^3). To create surface indents, the SMP was first heated to 65 °C in an oven. The SMP was taken out of the oven and a metal block with protruded surface features was immediately pressed onto the SMP surface. The manual pressing force was maintained until the sample was cooled down to room temperature (about 10 min under ambient condition). Afterward, the pressing force and the metal block were removed, marking the end of indentation deformation. Uniaxial stretching was introduced at 65 °C using dynamic mechanical analyzer (DMA 2980 manufactured by TA Instruments) and the deformation strains were fixed by cooling to 20 °C. Metallic thin films were deposited at 20 °C using a vacuum sputtering system (Denton Desk II) and the thickness was altered by varying the sputtering time. Strain recovery of the SMP/metal bilayer was conducted under a stress free condition in an oven at 65 °C.

Characterization. Scanning electronic microscopy (SEM) was conducted on HITACHI S-4800 microscope. Atomic force microscopy (AFM) characterization was conducted at room temperature in a contact mode using Dimension 3100 manufactured by Veeco. The wavelength and amplitude of wrinkles were obtained by measuring 70−80 individual wrinkles using the section analysis function in the Nanoscope software (Nanoscope 5.31r1). To determine the thickness of the metallic thin film on the SMP samples, a partially covered silicon wafer was sputtered under the identical condition for the SMP samples. The film thickness, which is the height difference between the coated and noncoated silicon wafer surfaces, was measured by AFM.

RESULTS AND DISCUSSIONS

A first set of localized wrinkles were created via the indentation method described in the Experimental Section and our previous paper, utilizing an Au/Pd alloy (1:1 ratio) as the rigid thin film.[17] This resulted in the localized lightly green color, shown as the upper image in Figure 1a. The area not affected by the indents remained dark, indicating no wrinkle formation. Following a typical shape memory cycle, a tensile strain of 5.7% was introduced via uniaxial stretching at 65 °C. Because of the Poisson effect, the tensile strain led to a compressive strain in the transverse direction, which created a second set of wrinkles. Consequently, a striking blue color was observed throughout the sample surface (the middle image in Figure 1a, obtained under typical laboratory ambient light condition). The blue color was preserved when the original stretching force was

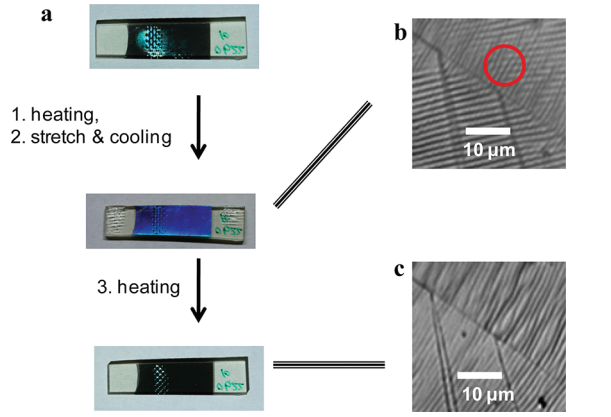

Figure 1. Demonstration of reversible and irreversible wrinkles on the same substrate. (a) The first locally green colored sample was created by the indentation method; following the arrow, the sample was heated, stretched, and cooled, which led to the uniform blue color; further down the arrow, heating erased the blue color, but the localized green colors remained. (b) The optical microscopic image of a local area where the uniaxial wrinkles (reversible) superimposed with the localized wrinkles from indent recovery (irreversible); the red circle identifies the diamond-shaped morphology. (c) The optical microscopic image of the same local area after heating, which erased the reversible wrinkle from the uniaxial stretching.

released after cooling to 20 °C, reflecting the unique character of SMP versus an elastomer substrate and the benefit of using an SMP for creating structural colors. The previously indented area, while still distinguishable from the rest of the area, no longer exhibited the green color, largely because it was overshadowed by the more intense blue color. Upon heating back to 65 °C, however, the strain due to the uniaxial stretching was released (erased). This led to disappearance of the blue color, whereas the light green color around the indents re-emerged (the bottom image in Figure 1a). The entire color changing process of Figure 1a can be repeated multiple times. We should note, however, that the specific colors described above are angle dependent due to their diffraction nature.[17] Thus, the "blue" and "green" colors are not fixed, they are used to facilitate the description of the spatial distribution of wrinkles and their appearance/disappearance at various stages in Figure 1a.

We further note that the upper and bottom images in Figure 1a are different in areas that are close but not in immediate proximity to the indents. Despite that, the macroscopic color changes in Figure 1a suggest that it is feasible to generate both reversible and irreversible wrinkles (and colors) on a single substrate. Comparison of the microscopic wrinkle structures (Figure 1b,c) confirms that the disappearance of the blue color in Figure 1a was indeed due to the removal of the second set of wrinkle, whereas the first set of localized wrinkle remained under the same condition. We should note that significant cracking in the metallic film are observed in both b and c in Figure 1. These microcracks, which do not exist in the as-deposited film, represent permanent structural defects that are irreversible. As such, the supposedly reversible wrinkle structure is not completely reversible at the microscopic scale. Further examination of the wrinkled surface containing both the reversible and irreversible wrinkles (Figure 1b) reveals that the overall surface morphology appears to be the superimposition of the two sets of wrinkles. In fact, diamond-shaped morphology (circled in red) is observed in certain regions. Such wrinkle morphology is not reported in the literature. However, similar square checkerboard morphology is considered energetically unfavorable over other morphologies such as herringbone morphology.[29] Thus, the two-step wrinkling method presented here may allow access to unique wrinkle morphologies, which we will explore further in the future. On the practical end, the existence of both reversible and irreversible structural colors on the same substrate offers unique opportunities for potential applications. For instance, the photos in Figure 1a imply a potential application as a smart label for temperature sensitive products. If the product has not been exposed to an elevated temperature, the label would appear blue throughout. If the product has been exposed to the elevated temperature, the label would show only the localized green colors.

We should note that wrinkle cracks are not always undesirable. In fact, studies have shown that formation of cracks could be helpful for the alignment of wrinkle structures.[30,31] More recently, Chung et al have demonstrated that the cracking densities of wrinkles can even be utilized to measure the strength of nanoscopic thin films.[32] In our particular case, however, cracking represents an obstacle to achieve high wrinkle reversibility at the microscopic scale. To understand the cracking behavior of wrinkles, in the following study, we focused on wrinkles generated by uniaxial stretch and replaced the alloy with gold as the thin film with the hope that the ductility of gold could alleviate the cracking issue. To further facilitate the study, we focused solely on uniaxial strains below.

In general, the compressive strain required for surface wrinkling may be created in two different modes, which are illustrated in Figure 2. Figure 2a shows mode I. The metal thin film is first deposited onto a nonstretched SMP surface at 20 °C. Subsequently, the SMP/metal bilayer is subject to a uniaxial stretching in the x direction at 65 °C. Because of the Poisson effect, the uniaxial tension in x direction leads to a compressive strain in the y direction. In Mode II (Figure 2b), the SMP substrate is first stretched in the x direction at 65 °C and the prestretch is fixed by cooling to 20 °C. The metal thin film is then deposited onto the prestretched SMP surface at 20 °C. Subsequently, the prestretch in the SMP is released upon heating back to 65 °C, leading to a compressive strain in the metal film in the x direction. Notably, the difference between the two modes lies in that the external mechanical deformation force is applied before (Mode II) and after (Mode I) the thin film deposition. As such, the localized wrinkle due to the indention (Figure 1a) corresponds to mode II, whereas the second set of wrinkle due to uniaxial stretching (Figure 1a) was created according to mode I.

We first studied the thin film cracking behavior for Mode I, by imposing different stretching forces in step 3 of Figure 2a. Various levels of uniaxial tensile strain along the x direction (ε_x) were introduced in the gold coated SMP samples. Figures 3a and 3b show the SEM and AFM images of a sample with a tensile strain of 4.1%. Cracks along the y direction (i.e., perpendicular to the tensile direction) are evident in both images. The AFM image shows clearly wrinkles perpendicular to the cracks in the vicinity of the cracks, but no wrinkles in the areas far away from the cracks. Cracking was also observed for a sample with ε_x as low as 2.6%, but not on the samples with ε_x less than 2.0%. Thus the critical tensile strain for cracking (not the critical buckling strain) is estimated to be around 2.0%. The low value of the critical cracking strain implies the difficulty in avoiding cracking for mode I. On a qualitative basis, we observed that the crack density increased with the tensile strain. In principle, such a correlation between crack density and tensile strain can be explored for measuring the tensile

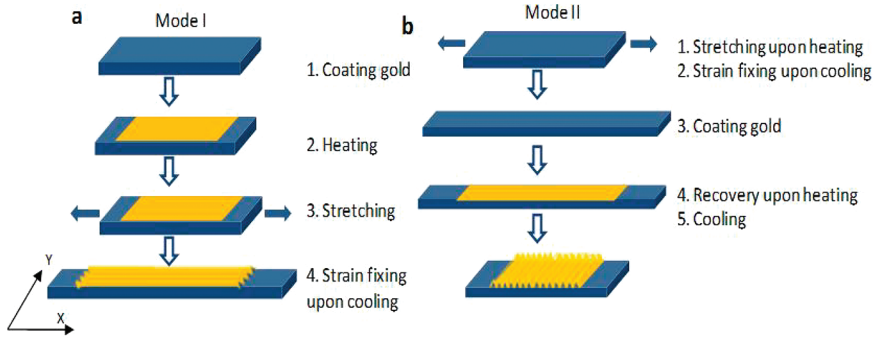

Figure 2. Wrinkle formation processes: (a) mode I, (b) mode II.

dx.doi.org/10.1021/am201727a | ACS Appl. Mater. Interfaces 2012, 4, 598–603

strength of the rigid thin films.[32] The wrinkle-based metrology, however, is outside the scope of the current work. We focus instead on identifying conditions to generate crack-free wrinkles.

In contrast to the ease of cracking for mode I, no cracks can be identified on a sample with a tensile strain of prestretch (ε_x) up to 13.5% for mode II (Figure 3c,d). The absence of cracking was confirmed by scanning through the entire surface using an optical interferometer. We should note that, in mode II, as the prestretch in the x direction is released upon shape recovery, a tensile strain is induced in the y direction ($\varepsilon_y > 0$) by Poisson's effect. With the SMP Poisson ratio of 0.45, the tensile strain follows: $\varepsilon_y = -0.45\varepsilon_x$, with ε_x being negative (compressive) due to release of the prestretch. Thus, the critical tensile strain for cracking appears to be at least 13.5% × 0.45 = 5.9% for mode II. Here, the cracking refers to the gold thin film. For the SMP used, the tensile strain of 13.5% at the prestretch approaches its strain-at-break. This makes it impossible to further extend the strain range in mode II to identify the critical cracking strain for the gold film. Despite that, it can be concluded that the critical cracking strain for mode II is much higher than that for mode I.

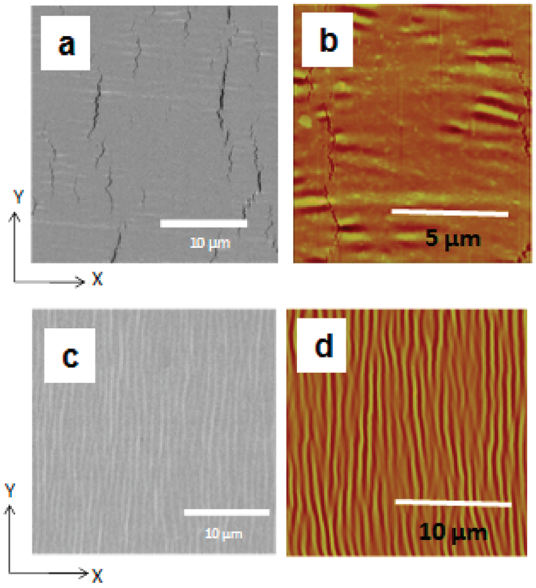

Figure 3. Morphology of the wrinkle surfaces. (a) SEM and (b) AFM images of a sample created according to mode I (ε_x = 4.1%); (c) SEM and (d) AFM images of a sample created according to mode II (ε_x = 3.9%). Gold film thickness is 18 nm in all cases.

At first glance, the drastically different cracking behaviors between the two modes appeared surprising. In both mode I and mode II, the compression to the thin film was created when the SMP was in the same heated state (i.e., rubbery state). That is, there was no difference in terms of the modulus of the substrate when wrinkling occurred. Further comparison between the two modes in Figure 2 revealed a key difference in the tensile stress in the metal film. In Mode I, wrinkling occurred (step 3 in Figure 2a) when an external force was applied to stretch the SMP, whereas no external force was present in the wrinkling step for Mode II (step 4 in Figure 2b). In both cases, the film is stressed biaxially. For the Mode I process, the metal film is deposited before the SMP substrate is stretched. Upon stretching, the film is strained in both x and y directions, with $\varepsilon_y = -\nu_s\ \varepsilon_x$ by Poisson effect. The strain is tensile in the x direction ($\varepsilon_x > 0$) and compressive in the y direction ($\varepsilon_y < 0$). Assuming the metal film to be linear elastic with Young's modulus E_f and Poisson's ratio ν_f, the stress components in the film are

$$\sigma_x = \frac{(1 - \nu_f\nu_s)E_f}{1 - \nu_f^2}\varepsilon_x \text{ and } \sigma_y = -\frac{(\nu_s - \nu_f)E_f}{1 - \nu_f^2}\varepsilon_x \quad (4)$$

Thus, the stress is tensile in the x direction ($\sigma_x > 0$) and compressive in the y direction ($\sigma_y < 0$), assuming $\nu_f < \nu_s$.

For the mode II process, the metal film is deposited on the prestretched SMP substrate. Upon heating, the strain in the substrate is relaxed because of the shape memory effect, and the metal film is subjected to compression in the x-direction ($\varepsilon_x < 0$). In this case, by eq 4, the stress is compressive in the x direction ($\sigma_x < 0$) but tensile in the y direction ($\sigma_y > 0$). Note that the compressive stress in mode I and the tensile stress in mode II both occur in the direction perpendicular to the stretch as a result of the mismatch in the Poisson's ratios of the film and the substrate. In particular, the tensile stresses in the film are drastically different for the two processes. With ν_f and ν_s being 0.42 and 0.45, respectively, the tensile stress for mode II is 27 times lower than that for Mode I at an identical strain level. Consequently, the film is unlikely to crack even with relatively large strain in the x-direction (ε_x) in mode II. Although the assumption of linear elasticity may not be valid for the current material system, the above stress analysis does offer a qualitative explanation on the origin of the drastically different thin film cracking behaviors for the two wrinkling modes. That is, despite the similarity between the two wrinkling modes, the tensile stress is significantly different, leading to drastic difference in the cracking behavior.

Another possible reason for the different cracking behaviors may be attributed to the dependence on the strain rate as reported previously.[7] For our system, there was indeed a large difference between the strain rates for mode I and mode II, calculated from the strain evolution curves recorded in the thermomechanical experiments. In mode I, the metal-coated SMP was stretched by applying a constant stretching force, which corresponds to a strain rate of 68%/min. In contrast, the strain (recovery) rate for mode II was only 3.9%/min. In principle, the different strain rates may have led to different cracking behaviors. To examine this possibility, an additional controlled mode I experiment was conducted in which the stretching force was gradually ramped to the target value with a corresponding strain rate of 3%/min. Even at this low strain rate, cracks were still present on the gold film. Hence, this controlled experiment confirmed that the strain rate effect is less significant for our system.

The crack-free behavior for mode II provides an ideal platform to further investigate the wrinkle mechanics without the uncertain impact of cracking. Wrinkled samples with different levels of prestretch and different film thicknesses were obtained and the wrinkle wavelengths and amplitudes were analyzed by AFM. Figure 4a shows that: (1) the wrinkle wavelength decreases with increasing strain of prestretch up to 5%; (2) beyond 5% prestretch, the wrinkle wavelength becomes approximately independent of strain. The dependence of the wrinkle wavelength on strain is evident through the direct comparison of the AFM images for two samples (Figure 5), showing more densely packed wrinkles on the sample with a 11.8% prestrain than the one with a 3.9% prestrain. The wrinkle amplitude, on the other hand, increases with the prestrain over the entire range (Figure 4b). Furthermore, for an identical prestrain, the general trend in panels c and d in Figure 4 reveals

dx.doi.org/10.1021/am201727a | ACS Appl. Mater. Interfaces 2012, 4, 598–603

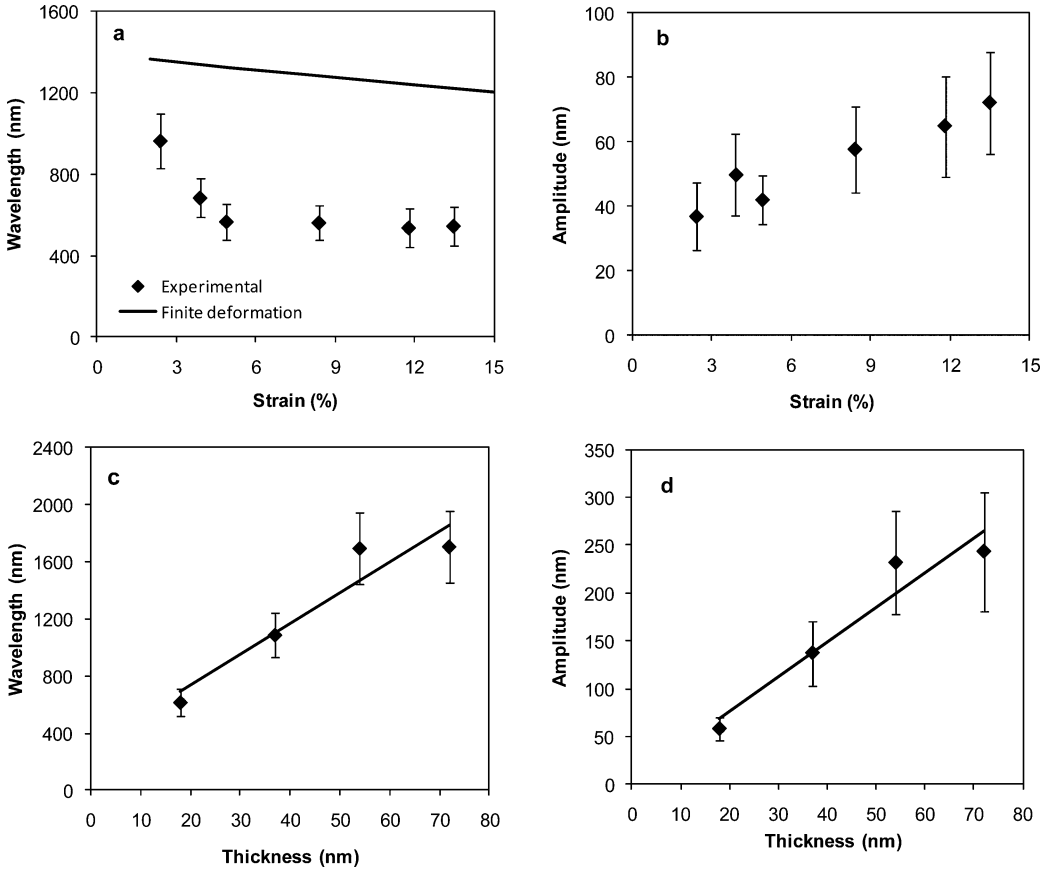

Figure 4. Wrinkle geometry created using mode II. Strain dependence of wrinkle (a) wavelength and (b) amplitude (film thickness = 18 nm); wrinkle (c) wavelength and (d) amplitude as a function of the film thickness (ε_x = 6.8%).

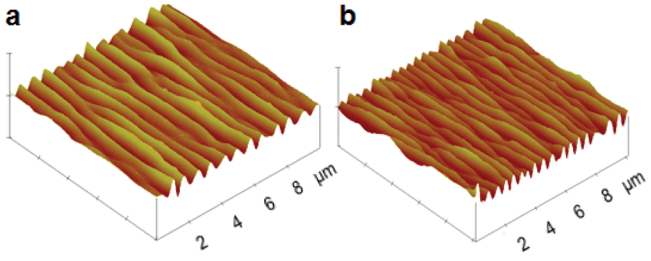

Figure 5. AFM three-dimensional micrographs of the wrinkled surfaces (film thickness = 18 nm). (a) ε_x = 3.9%, (b) ε_x = 11.8%.

that, within the experimental error, increasing the thin film thickness leads to increases in both the wrinkle wavelength and amplitude.

An important note to panels a and b in Figure 4 is that the wrinkle structures were characterized at 20 °C, which is below the T_g of the SMP. The SMP is essentially an elastomer above T_g with a modulus of 8.8 MPa, but it becomes significantly more rigid with a modulus of 2.9 GPa at room temperature. On the basis of the classical wrinkle theory (eq 2), one would anticipate that the wrinkle wavelength at a temperature above T_g of the SMP should be 6.9 times the wavelength at the room temperature for an identical sample. However, the wrinkle was formed at elevated temperature (above the T_g) and further change upon cooling should be considered postbuckling, for which eq 2 is no longer valid. Indeed, our measurements of the wrinkle wavelength for a representative sample showed that cooling and heating did not lead to any noticeable change in the wrinkle wavelength, whereas the amplitude did increase by 45% upon cooling. Such an increase in amplitude upon cooling was most likely due to the thermal strain generated upon cooling. When the system was cooled below the T_g, the wavelength/amplitude was locked in as the strain energy required for their change may have become too large to overcome. Given the complexity of the phase transition and the shape memory effect in the SMP as well as possible plastic deformation of the metal film, further mechanistic understanding of the wrinkling phenomenon in the SMP/metal bilayer system would benefit greatly from future theoretical modeling work.

The wavelength−strain relation in Figure 4a also deviates noticeably from eq 2, which predicts a constant wavelength independent of the strain. On the other hand, a finite deformation analysis by Jiang et al.[33] has predicted that the wrinkle wavelength decreases linearly with increasing strain over a large range (0−30%). Their prediction was found to be in excellent agreement with their experimental measurements using a system with single-crystal silicon ribbons bonded onto a prestretched elastomer substrate, where wrinkles were formed upon releasing the prestretch. We note several key differences in our system. First, the metal film in our system is more likely to deform plastically than the silicon ribbon. Second, while the SMP substrate behaves like an elastomer above T_g, the release of prestretch in our system was accompanied by a temperature change. Consequently, the wrinkling mechanism in our system may differ from the previous studies. As shown in Figure 4a, the wrinkle wavelength below the threshold strain of 5% decreases linearly but much more rapidly than the prediction by the finite deformation theory of Jiang et al.[33] More strikingly, the wrinkle wavelength becomes

dx.doi.org/10.1021/am201727a | ACS Appl. Mater. Interfaces 2012, 4, 598−603

independent of the strain above the threshold strain of 5%, in sharp contrast with the finite deformation theory. We suspect that the nonlinear stress−strain behavior of the Au thin film (e.g., plasticity) may play an important role in the observed wrinkling behavior. The stress−strain curves of the Au thin films in our systems (thickness 18−80 nm) are not reported in the literature. However, a study by Espinosa and Prorok suggested that the mechanical properties of gold thin films (thickness >0.3 μm) are indeed nonlinear even at strains as low as 1%.[34] Thus, the wrinkle behavior in Figure 4a calls for new understanding of the mechanics that takes into account the nonlinear mechanical properties of the thin film supported on a modulus changing shape memory polymer.

For a qualitative understanding on the effect of plasticity, a simple model is briefly described as follows. The main assumption of this model is that partial yielding of the wrinkled Au film leads to the nonlinearity of the wavelength-strain relation shown in Figure 4a. When the prestrain reaches a critical value (i.e., the yield strain of Au), part of the Au film will yield and deform plastically with a smaller tangential modulus than the elastic modulus before yielding. In other words, the "effective" modulus of the Au film is reduced due to partial plastic yielding. Below the threshold strain of 5%, a higher prestrain should result in a higher fraction of the yielded Au film. As such, the effective modulus of the Au film should decrease with the prestrain. By eq 2, the wrinkle wavelength should decrease with increasing strain. This trend continues until the prestrain reaches the threshold strain when the entire Au film (including the wrinkle peak and valley) yields and deforms plastically. Beyond the threshold strain, the "effective" modulus of the film becomes independent of the prestrain and hence a constant wavelength as shown in Figure 4a. The details of this model will be presented in another paper.

CONCLUSION

Utilizing a metallic layer as the thin film, the unique aspects of SMP (relative to elastomers) as a wrinkle substrate were investigated. Two different wrinkling modes were employed to create the in-plane compression required for wrinkle formation: metal deposition onto an SMP followed by stretching (mode I); metal deposition onto a prestretched SMP followed by releasing the tensile prestrain (mode II). Whereas thin film cracking occurred at tensile strains as low as 2.6% for mode I, no cracks were observed at tensile prestrains as high as 13.5% for mode II. The drastically different cracking behaviors were attributed to the large difference in the tensile stresses in the metal films. Utilizing both wrinkling modes in the same process, reversible and irreversible wrinkles (and associated diffraction colors) were created on a single SMP substrate. Quantitative characterization of the crack-free wrinkles (mode II) suggests that the wrinkle wavelength decreases with strain at strains between 2 and 5%, but becomes approximately independent of strain at strains above 5%. This wrinkling behavior is in sharp contrast with the existing theory assuming elastic behavior for the film and the substrate. As such, a new mechanics model will need to be developed in the future by considering the unique thermomechanical properties of the shape memory substrate and the nonlinear mechanical response of the gold thin film.

AUTHOR INFORMATION

Corresponding Author

*Fax: +1 586 986 1207. Tel: +1 586 947 2471. E-mail: tao.xie@gm.com.

ACKNOWLEDGMENTS

The authors thank Mr. Curtis Wong for SEM characterization.

REFERENCES

(1) Schweikart, A.; Fery, A. *Microchim. Acta* **2009**, *165*, 249.
(2) Chung, J.; Nolte, A.; Stafford, C. *Adv. Mater.* **2011**, *23*, 349.
(3) Yang, S.; Khare, K.; Lin, P. *Adv. Funct. Mater.* **2010**, *20*, 2550.
(4) Genzer, J.; Groenewold, J. *Soft Matter* **2006**, *2*, 310.
(5) Khang, D. Y.; Rogers, J. A.; Lee, H. H. *Adv. Funct. Mater.* **2009**, *19*, 1526.
(6) Bowden, N.; Brittain, S.; Evans, A.; Hutchinson, J.; Whitesides, G. *Nature* **1998**, *393*, 146.
(7) Efimenko, K.; Rackaitis, M.; Manias, E.; Vaziri, A.; Mahadevan, L.; Genzer, J. *Nat. Mater.* **2005**, *4*, 293.
(8) Efimenko, K.; Finlay, J.; Callow, M. E.; Callow, J. A.; Genzer, J. *ACS Appl. Mater. Interface* **2009**, *1*, 1031.
(9) Torres, J. M.; Stafford, C. M.; Vogt, B. D. *Polymer* **2010**, *51*, 4211.
(10) Torres, J. M.; Stafford, C. M.; Vogt, B. D. *ACS Nano* **2009**, *3*, 2677.
(11) Huang, J.; Juszkiewicz, M.; de Jeu, W.; Cerda, E.; Emrick, T.; Menon, N.; Russell, T. P. *Science* **2007**, *317*, 650.
(12) Chan, E.; Smith, E.; Hayward, R.; Crosby, A. *Adv. Mater.* **2008**, *20*, 711.
(13) Chung, J.; Nolte, A.; Stafford, C. M. *Adv. Mater.* **2009**, *21*, 1358.
(14) Chan, E.; Crosby, A. *Adv. Mater.* **2006**, *18*, 3238.
(15) Lin, P.; Vajpayee, S.; Jagota, A.; Hui, C.; Yang, S. *Soft Matter* **2008**, *4*, 1830.
(16) Lin, P.; Yang, S. *Soft Matter* **2009**, *5*, 1011.
(17) Xie, T.; Xiao, X.; Li, J.; Wang, R. *Adv. Mater.* **2010**, *22*, 4390.
(18) Schweikart, A.; Pazos-Perez, N.; Alvarez-Puebla, R.; Fery, A. *Soft Matter* **2011**, *7*, 4093.
(19) Zhao, Y.; Huang, W. M.; Fu, Y. Q. *J Micromech. Microeng.* **2011**, *21*, 067007.
(20) Fu, C.; Grimes, A.; Long, M.; Ferri, C.; Rich, B.; Ghosh, S.; Lee, L.; Gopinathan, A.; Khine, M. *Adv. Mater.* **2009**, *21*, 4472.
(21) Stafford, C.; Harrison, C.; Beers, K.; Karim, A.; Amis, E.; Vanlandingham, M.; Kim, H.; Volksen, W.; Miller, R.; Simonyi, E. *Nat. Mater.* **2004**, *3*, 545.
(22) Chung, J.; Chastek, T.; Fasolka, M.; Ro, H.; Stafford, C. *ACS Nano* **2009**, *3*, 844.
(23) Lin, P.; Yang, S. *Appl. Phys. Lett.* **2007**, *90*, 241903.
(24) Xie, T. *Nature* **2010**, *464*, 267.
(25) Xie, T. *Polymer* **2011**, *52*, 4895.
(26) Mather, P.; Luo, X.; Rousseau, I. *Annu. Rev. Mater. Res* **2009**, *39*, 445.
(27) Lendlein, A.; Kelch, S. *Angew. Chem., Int. Ed.* **2002**, *41*, 2034.
(28) Xie, T.; Rousseau, I. *Polymer* **2009**, *50*, 1852.
(29) Cai, S.; Braid, D.; Crosby, A. J.; Suo, Z.; Hutchinson, J. W. *J. Mech. Phys. Solids* **2011**, *59*, 1094.
(30) Rand, C.; Sweeney, R.; Morrissey, M.; Hazel, L.; Crosby, A. *Soft Matter* **2008**, *4*, 1805.
(31) Douville, N. J.; Li, Z. Y.; Takayama, S.; Thouless, M. D. *Soft Matter* **2011**, *7*, 6493.
(32) Chung, J. Y.; Lee, J. H.; Beers, K. L.; Stafford, C. M. *Nano Lett.* **2011**, *11*, 3365.
(33) Jiang, H. Q.; Khang, D. Y.; Song, J. Z.; Sun, Y. G.; Huang, Y. G.; Rogers, J. A. *Proc. Natl. Acad. Sci. U.S.A.* **2007**, *104*, 15607.
(34) Espinosa, H.; Prorok, B. *J. Mater. Sci.* **2003**, *38*, 4125.